Journal of Coupled Systems and Multiscale Dynamics

doi:10.1166/jcsmd.2015.1063
J. Coupled Syst. Multiscale Dyn.
Vol. 3(1)/2330-152X/2015/038/009

Research Article

Theoretical analysis of the relationship between changes in retinal blood flow and ocular perfusion pressure

Simone Cassani[1], Alon Harris[2], Brent Siesky[2], and Julia Arciero[1,*]

[1]*Department of Mathematical Sciences, IUPUI, Indianapolis, 46202, IN*
[2]*Department of Ophthalmology, Glick Eye Institute, Indiana University School of Medicine, Indianapolis, 46202, IN*

(Received: 7 November 2014. Accepted: 7 January 2015)

ABSTRACT

Impaired retinal perfusion and blood flow regulation are associated with many ocular and systemic diseases such as glaucoma, age-related macular degeneration, and diabetes. Identifying the physiological conditions that lead to deficient circulation will improve the understanding of these disease processes. Here, a mathematical model is used to predict how retinal blood flow changes as mean arterial pressure (MAP) and/or intraocular pressure (IOP) are varied. The model used in this study couples two previously developed models to simulate blood flow through the retinal vasculature, which is represented by compartments for the central retinal artery (CRA), large arterioles, small arterioles, capillaries, small venules, large venules, and the central retinal vein (CRV). As a result of coupling the two previously developed models, the effects of pressure in the CRA and CRV are included as well as a mechanistic description of blood flow autoregulation in the microcirculation of the retina. The nonlinear effect of this coupling on the pressure drops throughout the network is shown, and the model predicted values of flow for increased pressure values are compared with laser Doppler flowmetry measures in rats and cats, showing good agreement during MAP and/or IOP elevation.

Keywords: Blood Flow, Retina, Computational Modeling, Pressure, Autoregulation, Coupled Problems.
Section: Life, Climate & Environmental Sciences

1. INTRODUCTION

Several ocular diseases, including glaucoma and age-related macular degeneration, have been associated with impaired retinal perfusion.[1–6] Although multiple risk factors contribute to these diseases, understanding the conditions that affect the normal supply of blood flow to retinal tissue is likely to provide important insight into the underlying mechanisms for these diseases and to aid in identifying new therapeutic approaches for them.

Changes in ocular perfusion pressure (OPP), which is a measure that accounts for both mean arterial pressure (MAP) and intraocular pressure (IOP) and is calculated as 2/3∗MAP-IOP, can alter retinal blood flow and consequently retinal function.[5–7] For example, He et al.[7] recently showed that decreases in OPP due to increases in IOP led to progressively attenuated levels of both retinal function and blood flow.

When retinal tissue exhibits normal vascular autoregulation, blood flow is maintained relatively constant despite changes in intraocular and intravascular pressure dynamics. This homeostasis in blood flow contributes to the normal functioning of the retinal. In the retina,

∗Author to whom correspondence should be addressed.
Email: jarciero@math.iupui.edu

several mechanisms of blood flow regulation, such as myogenic,[8,9] shear,[10] metabolic,[11,12] and carbon dioxide responses,[13] have been shown to combine to achieve this relatively constant level of blood flow for a large range of MAP (60–100 mmHg) when IOP is held at a normal level (10–15 mmHg). If some of these mechanisms are impaired, the autoregulation plateau in blood flow may be reduced or lost, possibly leading to decreased oxygenation of the retina. It has also been observed that changes in IOP can alter the mechanical load on retinal neurons[7,14–16] and could compromise retinal function without having a direct effect on blood flow. Interestingly, there is evidence that reduced blood flow outside the range of autoregulation does not always impair retinal function, suggesting that other mechanisms are present to maintain retinal function even when autoregulation is not functioning. Several studies[17–20] have proposed that increases in the amount of oxygen extracted per unit arterial blood flow help to compensate for the reduced blood supply to retinal tissue, likely preserving retinal function.

He et al. recently provided both qualitative[21] and quantitative[7] descriptions of the relationship between retinal function, blood flow, oxygen extraction ratio, and mechanical stress. They performed a combined experimental and theoretical study in which they simultaneously measured retinal function, blood flow, and tissue oxygen tension in Long-Evans rats over a wide range of controlled IOP values and developed a mathematical model relating blood flow to retinal function across a range of OPP values. However, their model is based on a number of assumptions and does not provide a mechanistic explanation for the observed changes in blood flow and retinal function. For example, the relationship between oxygen extraction and blood flow is assumed to follow an exponentially decaying function based on data from brain since data in the retina is not available. Also, a simple linear threshold function is defined to describe the relationship between IOP and the mechanical load due to IOP. While these empirical relationships support the data, they are not generated according to the underlying physical mechanisms of the system.

In this study, a hemodynamic model that accounts for the biomechanical action of IOP on blood flow through the central retinal vessels and retinal microvasculature[22] is coupled to a vessel wall mechanics model of blood flow autoregulation in the retinal microcirculation.[23] Predictions of blood flow and oxygen delivery to the retina in the uncoupled and coupled models are compared, and it is hypothesized that the mechanical effects of IOP are necessary to yield model results that accurately predict the measured levels of ocular blood flow previously obtained in experiments.[7,24] Ultimately, this biomechanical model provides a physical description of hemodynamics in the retina that will help to illustrate the roles of vascular and mechanical factors that may contribute to multiple ocular diseases.

2. METHODS

2.1. Model Coupling

Blood supply to the retina is simulated using a mathematical model that describes the hemodynamic and mechanical properties of multiple vessel compartments, as depicted in Figure 1. The model is analogous to an electrical circuit in which blood is propelled through the system by a pressure gradient and the vessels are modeled as a network of resistors, representing the resistance to blood flow offered by the system. An analogy to Ohm's Law is used to describe the blood flow (Q) through the system: $Q = \Delta P/R$, where ΔP represents the pressure difference along a vessel and R is the vascular resistance.

The model used in this study is developed by coupling two previously developed mathematical models of the retinal circulation. The first model, described in Ref. [23] (herein referred to as the *microcirculation model*), is used to model the blood flow through the large arterioles (LA), small arterioles (SA), capillaries (C), small venules (SV), and large venules (LV) according to passive and active length-tension characteristics of vascular smooth muscle. This wall mechanics model accounts for retinal autoregulation generated by myogenic, shear, metabolic, and CO_2 mechanisms. These mechanisms lead to changes in vascular smooth muscle tone and hence vessel diameter as changes in pressure, shear stress, and metabolites are sensed.

The second model, described in Ref. [22] (herein referred to as the *macrocirculation model*), simulates blood flow upstream, within, and downstream of the microcirculation. In particular, the macrocirculation model implements mechanical principles to describe blood flow through the central retinal artery (CRA) and the central retinal vein (CRV). Although both models separately provide insight into key aspects of retinal blood flow regulation, the macrocirculation model is limited by using a phenomenological description of autoregulation, and the microcirculation model is limited by describing only the dynamics in the retinal microcirculation.

In the present study, the microcirculation and macrocirculation models are combined into a single *coupled model* that includes a mechanistic description of blood flow autoregulation in the microcirculation as well as the effects of IOP on the CRA and CRV. The physical coupling of the models occurs at the $P_{1,2}$ node between the CRA and LA and the $P_{4,5}$ node between the LV and CRV (see Fig. 1). In this way, the coupling substitutes the phenomenological approach in Ref. [22] with the mechanistic one used in Ref. [23], providing a more accurate description of the autoregulatory ability of the retina in a full

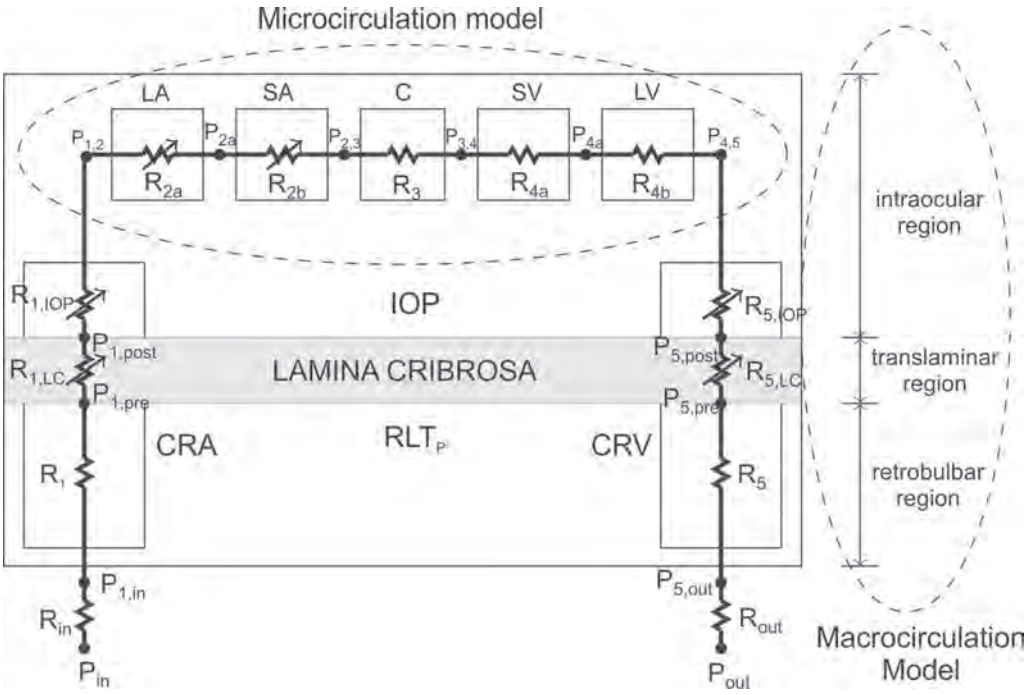

Fig. 1. Schematic for retinal vascular network in the coupled model. The vasculature is divided into seven compartments: the central retinal artery (CRA), large arterioles (LA), small arterioles (SA), capillaries (C), small venules (SV), large venules (LV), and central retinal vein (CRV). Each compartment is modeled as a resistor (R). The retinal vasculature supply flows through three regions: the intraocular region, translaminar region, and retrobulbar region. The intraocular segments are exposed to IOP, the translaminar segments are exposed to an external pressure that depends on stress in the lamina cribrosa (shaded gray), and the retrobulbar segments are exposed to the retrolaminar tissue pressure (RLTp). Resistors marked with arrows indicate that their diameters change either passively (due to IOP) or actively (due to autoregulation). Dashed circled regions indicate the two previous models (the microcirculation model[23] and the macrocirculation model[22]) that are combined in the current study to form the coupled model.

retinal vascular model that also includes the hemodynamics in the vessels that supply (CRA) and drain (CRV) the retina. A complete description of the two original (i.e., uncoupled) models can be found in Ref. [23] (microcirculation model) and Ref. [22] (macrocirculation model). In this study, the relevant features of and changes to these two models necessary to generate the combined model will be discussed.

As in the previous two models, the coupled model is characterized by both variable and fixed resistances. The resistances R_{in} and R_{out} describe the blood vessel resistance upstream of the CRA and downstream of the CRV. Variable resistances are marked with an arrow in Figure 1, and the remaining resistances are fixed. Resistances R_{2a} and R_{2b} are vasoactive resistances that change according to autoregulation mechanisms in the system. Resistances $R_{1,\text{LC}}$, $R_{1,\text{IOP}}$, $R_{5,\text{IOP}}$ and $R_{5,\text{LC}}$ are passive resistances that change according to the Law of Laplace (see Ref. [22]) due to the external pressure of the IOP in the intraocular region and the mechanical stress exerted by the lamina cribrosa on the CRA and the CRV in the translaminar region (see Fig. 1). Additional details on the effects of the lamina cribrosa compression on the system can be found in Refs. [22, 25].

Conservation of flow in the network yields the following nonlinear system of equations:

$$\begin{cases} \dfrac{P_{\text{in}}-P_{1,\text{post}}}{R_{\text{in}}+R_1+R_{1,\text{LC}}(\bar{P})}-\dfrac{P_{1,\text{post}}-P_{1,2}}{R_{1,\text{IOP}}(\bar{P})}=0 \\ \dfrac{P_{1,\text{post}}-P_{1,2}}{R_{1,\text{IOP}}(\bar{P})}-\dfrac{P_{1,2}-P_{4,5}}{R_{2a}(\bar{P},D,A)+R_{2b}(\bar{P},D,A)+R_3+R_{4a}+R_{4b}}=0 \\ \dfrac{P_{1,2}-P_{4,5}}{R_{2a}(\bar{P},D,A)+R_{2b}(\bar{P},D,A)+R_3+R_{4a}+R_{4b}} \\ \quad -\dfrac{P_{4,5}-P_{5,\text{post}}}{R_{5,\text{IOP}}(\bar{P})}=0 \\ \dfrac{P_{4,5}-P_{5,\text{post}}}{R_{5,\text{IOP}}(\bar{P})}-\dfrac{P_{5,\text{post}}-P_{\text{out}}}{R_{5,\text{LC}}(\bar{P})+R_5+R_{\text{out}}}=0 \end{cases} \tag{1}$$

where the definitions of the pressures (P) and resistances (R) are shown in Figure 1. The four variables of the system are given in the vector $\bar{P}=[P_{1,\text{post}}, P_{1,2}, P_{4,5}, P_{5,\text{post}}]$. The value of P_{out} is fixed at 14 mmHg, while the value of P_{in} is varied in the different simulations. Some of the vascular resistances depend on the pressure values (indicated in Eq. (1) by an explicit dependence in parentheses), while the remaining resistances are constant and equal to

their control state values listed in Tables II–III. R_{2a} and R_{2b} also depend on the diameter (D) and smooth muscle activation (A) values solved in Eq. 2. Of note, the coupled model differs from the macrocirculation model because it focuses only on the steady state solution instead of on time-dependent dynamics.

The following equations are solved for the steady state diameter and smooth muscle activation of the LA and SA according to the four autoregulation mechanisms:

$$\begin{cases} \dfrac{dD_i}{dt} = \dfrac{1}{\tau_d}\dfrac{D_c}{T_c}(T_i - T_{\text{total}}) \\ \dfrac{dA_i}{dt} = \dfrac{1}{\tau_a}(A_{\text{total}} - A_i) \end{cases} \quad i = \text{LA, SA} \tag{2}$$

where D_i and A_i are the diameter and level of smooth muscle activation, respectively. Constants $\tau_d = 1$ s and $\tau_a = 1$ min are the characteristic time constants regulating the changes in diameter and smooth muscle activation, and D_c and T_c are constants. The tension generated in the vessel wall according to the Law of Laplace is given by $T_i = (P_i - \text{IOP})D_i/2$. The model representation for vessel wall tension, $T_{\text{total}} = T_{\text{pass}} + A_{\text{total}}T_{\text{active}}$, is the sum of a passive component (T_{pass}) that arises from the structural elements of the vessel and a maximally active component (T_{active}) that arises from the constriction or relaxation of vascular smooth muscle. The passive component is assumed to be an exponential function of diameter, and the maximally active component is modeled as a Gaussian function of vessel diameter. To obtain the active component of tension in the vessel wall, the maximally active tension is multiplied by A_{total}, which is a sigmoidal function (Eq. (3)) that varies between 0 and 1 and that depends on a stimulus function (S_{tone}, Eq. (4)) that determines the degree of vascular smooth muscle constriction:

$$A_{\text{total}} = \frac{1}{1 + \exp(-S_{\text{tone}})} \tag{3}$$

$$S_{\text{tone}} = C_{\text{myo}}T - C_{\text{shear}}\tau - C_{\text{meta}}S_{\text{CR}} - C_{\text{CO}_2}S_{\text{CO}_2} + C''_{\text{tone}} \tag{4}$$

The stimulus function is a linear combination of the myogenic, shear-dependent, metabolic, and carbon dioxide autoregulation mechanisms (for details, see Ref. [23]). The metabolic response depends on the oxygen saturation level in blood. The model is used to calculate this oxygen saturation level as in Ref. [23], in which a Krogh-type cylinder model is used to define oxygen diffusion into tissue. Oxygen is assumed to be delivered by the LA, SA, and C compartments but is neglected in the SV and LV compartments. Oxygen demand in the tissue is assumed constant.

Once the vessel diameter (D) is determined for the LA and SA, the values of the resistances R_{2a} and R_{2b} can be computed using Poiseuille's Law:

$$R = \frac{128L\mu}{\pi n D^4} \tag{5}$$

where L is vessel length, μ is blood viscosity, and n is the number of vessels in the compartment.

2.2. Control State

A control (or reference) state represents conditions in a healthy eye. As in Ref. [22], the control state value of IOP is 15 mmHg, and the control state value of RLTp is 7 mmHg. The control state values of $P_{\text{in}} = 62.2$ mmHg and $P_{\text{out}} = 14$ mmHg are determined in the coupled model according to Color Doppler Imaging data as in Ref. [22].

To compute the control state value of R_{in} and R_{out}, the control state for the uncoupled model is first computed as in Ref. [23] using the value of $P_{1,2}$ and $P_{4,5}$ from Ref. [22]. Then, the pressure drop between the nodes $P_{1,2}$ and $P_{1,\text{in}}$, and between the nodes $P_{4,5}$ and $P_{5,\text{out}}$ is computed using Ohm's Law. The value of R_{in} and R_{out} is equal to $R_{\text{in}} = (P_{\text{in}} - P_{1,\text{in}})/Q_{\text{un}}$ and $R_{out} = (P_{5,\text{out}} - P_{\text{out}})/Q_{\text{un}}$, where all the quantities are equal to their control state value and Q_{un} is the value of blood flow in the control state of the uncoupled model.

The procedure used to compute the control state is iterative and is based on many of the control state assumptions in Refs. [22, 23]. First, the pressure values for $P_{1,2}$ and $P_{4,5}$ are set to the same values as in Ref. [22] (providing an initial guess), and then pressure drops across LA, SA, C, SV, and LV are computed as in Ref. [23]. The control state values of the LA and SA diameters are obtained by solving (2), assuming that $A_{\text{LA}} = A_{\text{SA}} = 0.5$ in the control state. The control state value of the capillary diameter is assumed to be 6 μm, and a symmetry condition that dictates the length and number of vessels in each compartment is used to determine the control state diameter values of the SV and LV.[23] The flow in each compartment is computed using Poiseuille's Law, and then the remaining geometric parameters, numbers, and lengths of the vessels in each compartment are computed.[23] A comprehensive list of the geometric and mechanical parameters characterizing the CRA and CRV are given in Ref. [22].

Once the vascular network geometry for the model is determined, the control state resistance for each compartment is computed using Poiseuille's Law (Eq. 5). System (1) is then solved to compute the control state for the coupled model. The values of $P_{1,2}$ and $P_{4,5}$ for the coupled model are compared with the initial guess. The iterations cease when the difference between the initial guess and the computed value is within a certain tolerance. If the condition on the tolerance is not satisfied, the predicted value is set as the new initial guess and the process is repeated. All control state values and parameters for the coupled model are listed in Tables I–III.

2.3. Simulation Procedure

In this study, simulations are run for two different versions of the model: an uncoupled version (microcirculation model) and the new coupled model defined here. The procedure used to solve the coupled model is the same as

Table I. Control state values for retinal vascular network compartments.

	CRA	LA	SA	C	SV	LV	CRV
Diameter, μm							
Retrobulbar	175	–	–	–	–	–	238
Translaminar	174.73	–	–	–	–	–	238.76
Intraocular	173.64	105.54	48.07	6	69.66	155.70	235.18
Length (total), mm	10	5.86	4.27	0.54	4.27	5.86	10
Retrobulbar	8.8	–	–	–	–	–	8.8
Translaminar	0.2	–	–	–	–	–	0.2
Intraocular	1	5.86	4.27	0.54	4.27	5.86	1
Number of segments, n	1	4	38	191172	38	4	1
Wall thickness, μm	39.72	–	–	–	–	–	10.72
Pressure drop, mmHg	5.96	4.99	7.99	4.02	1.84	1.13	1.88
Blood viscosity, cP	3.00	2.28	2.06	10.01	2.09	2.44	3.24
Shear stress, dyn/cm^2							
Retrobulbar	34.64	–	–	–	–	–	14.87
Translaminar	34.80	–	–	–	–	–	14.73
Intraocular	35.46	30	30	15	10	10	15.41
Velocity, cm/s							
Retrobulbar	2.53	–	–	–	–	–	1.37
Translaminar	2.53	–	–	–	–	–	1.36
Intraocular	2.57	1.74	0.88	0.01	0.42	0.80	1.40

the procedure described to compute the control state. The two different versions of the model are used to predict the blood flow, blood oxygen saturation, and $P_{1,2}$ and $P_{4,5}$ values for MAP = 20–165 mmHg and IOP = 7.5–31 mmHg. A comparison between the results of the coupled and uncoupled models is presented along with corresponding experimental measurements from rats[7, 21] and cats.[24]

3. RESULTS

3.1. Effect of Model Coupling

The effect of coupling the microcirculation and macrocirculation models is depicted in Figure 2 by comparing the uncoupled microcirculation model (black curves) and coupled model (blue curves) predictions for $P_{1,2}$ and $P_{4,5}$ (panel A), the pressure drop along the CRA (panel B), and the total CRA resistance (panel C) as MAP is varied between 65 and 165 mmHg and IOP = 15 mmHg. A few key assumptions differ between the uncoupled and coupled models. For example, in the uncoupled model, $P_{4,5}$ is held fixed (Fig. 2(A)). Also, the pressure drop along the CRA (i.e., $\Delta P_{\text{CRA}} = P_{\text{in}} - P_{1,2}$) in the uncoupled model is assumed constant (Fig. 2(B)), whereas the pressure drop along the CRA in the coupled model varies according to the effects of the IOP-RLTp pressure gradient and laminar effects on the CRA. Total resistance in the CRA is computed according to Ohm's Law as $R_{CRA} = (P_{\text{in}} - P_{1,2})/Q$, where Q is the retinal blood flow through the system.

Together, the panels in Figure 2 provide a mechanical rationale for why the model predictions for the uncoupled and coupled model differ substantially. In Figure 3, the predictions for flow and venous oxygen saturation are compared for the two different models. In both cases, tissue oxygen demand is assumed to be held constant at 1 cm^3 O_2/100 cm^3/min, MAP ranges from 65 to 165 mmHg, and IOP = 15 mmHg.

In Figure 4, the various mechanisms of autoregulation are turned "on" and "off" to demonstrate which mechanisms contribute most significantly to generating the autoregulation plateau in the coupled model. Consistent with the findings in Ref. [23], these results show that the metabolic and carbon dioxide mechanisms are most important for achieving autoregulation.

Table II. Pressure values at each network node in the control state.

Node	Pressure, mmHg	Node	Pressure, mmHg
P_{in}	62.22	$P_{3,4}$	22.97
$P_{1,\text{in}}$	45.94	P_{4a}	21.14
$P_{1,\text{pre}}$	40.71	$P_{4,5}$	20.01
$P_{1,\text{post}}$	40.60	$P_{5,\text{post}}$	19.81
$P_{1,2}$	39.98	$P_{5,\text{pre}}$	19.78
P_{2a}	34.99	$P_{5,\text{out}}$	18.13
$P_{2,3}$	27.00	P_{out}	14

Table III. Resistance values for each vessel compartment at control state.

Segment	Resistance, mmHg/(ml/s)	Segment	Resistance, mmHg/(ml/s)
R_{in}	2.68e4	R_{4a}	3.03e3
R_1	8.60e3	R_{4b}	1.86e3
$R_{1,\text{LC}}$	1.97e2	$R_{5,\text{IOP}}$	3.24e2
$R_{1,\text{IOP}}$	1.01e3	$R_{5,\text{LC}}$	6.09e1
R_{2a}	8.21e3	R_5	2.70e3
R_{2b}	1.32e4	R_{out}	6.80e3
R_3	6.63e3		

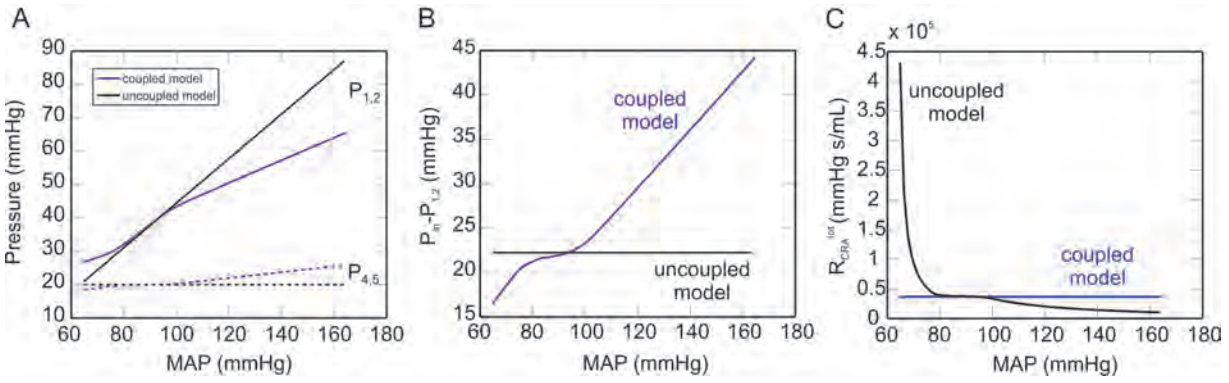

Fig. 2. (A) Model predicted values of $P_{1,2}$ (solid) and $P_{4,5}$ (dashed) for the uncoupled model (black curves) and coupled model (blue curves). (B) Pressure drop along the CRA for the uncoupled model (black curve) and coupled model (blue curve). (C) Total resistance in the CRA in the uncoupled model (black curve) and coupled model (blue curve). In all panels, MAP is varied between 65 and 165 mmHg and IOP = 15 mmHg.

3.2. Comparison with Experimental Measurements

To explore which version of the theoretical model (coupled or uncoupled) provides a better depiction of reality, model predictions are compared with experimental measurements from rats[7,21] and cats.[24] In Figure 5, normalized values of blood flow are predicted in both the coupled and uncoupled models and compared with data from Refs. [7, 21, 24] as MAP is varied between 20 and 165 mmHg for IOP = 10 mmHg.

He et al.[7,21] measure blood flow in rat retina at low-, normal- and elevated-blood pressure values corresponding to MAP = 59, 108, and 156 mmHg, respectively, as IOP is varied over a range of 10–110 mmHg. The coupled and uncoupled models are only capable of handling IOP values between 7.5 and 31 mmHg, and these results are compared with the findings from Refs. [7, 21] in Figure 6. In the case of low MAP, as IOP increases, the diameter of the small arterioles decreases until the point of collapse, yielding the observed absence of blood flow when IOP > 22 mmHg (red, solid curve, Fig. 6).

4. DISCUSSION

The vascular model of the retina developed in this study incorporates the mechanical effects of IOP and four autoregulation response mechanisms to describe blood flow to the retina. The blood flow predicted by the coupled model is significantly closer to pressure-flow experimental data collected by He et al.[7,21] and Tani et al.[24] than blood flow levels predicted by the uncoupled model, supporting the improvements offered by the coupled model over the uncoupled model. The coupled model could be further improved upon by modeling the venules as Starling resistors and thereby allowing venous collapse for very high IOP values (as in Ref. [22]) and by implementing a more heterogeneous vascular network geometry in the retina (e.g., using a Green's function modeling approach as in Ref. [26]). Nevertheless, the excellent agreement between the flow versus pressure predictions using the coupled model and experimental data from Refs. [7, 21, 24] provides confidence in the model assumptions and equations.

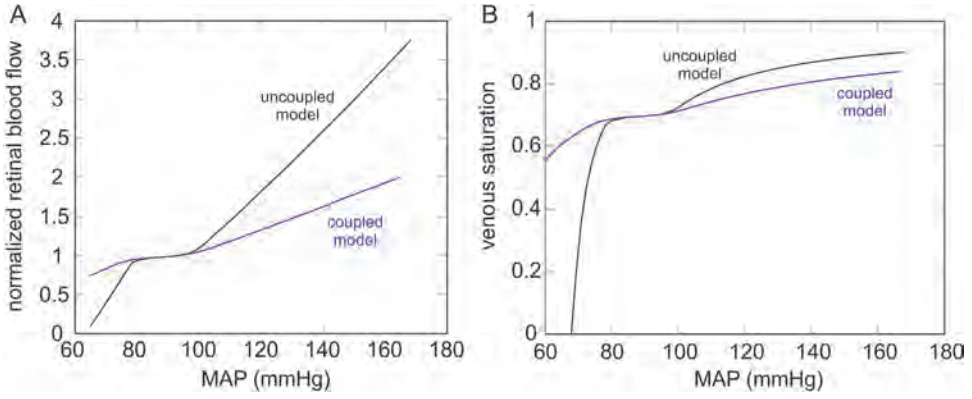

Fig. 3. (A) Predicted values of retinal blood flow (normalized) as MAP is varied (65–165 mmHg) using the uncoupled model (black curve) and coupled model (blue curve). (B) Predicted values for venous oxygen saturation as MAP is varied (65–165 mmHg) using the uncoupled model (black curve) and coupled model (blue curve). Arterial venous oxygen saturation was assumed to be 0.97 and tissue oxygen demand is assumed to be held constant at 1 cm^3 O_2/100 cm^3/min. In both panels, IOP = 15 mmHg.

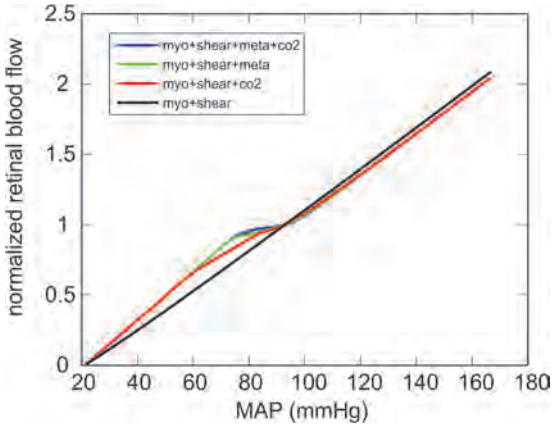

Fig. 4. Model predicted values of retinal blood flow (normalized) as MAP is varied (20–165 mmHg) using the coupled model. Autoregulation mechanisms are turned on and off to assess their individual contributions. The following combinations are included: all mechanisms (blue curve), myogenic + shear + metabolic (green curve), myogenic + shear + CO_2 (red), myogenic + shear (black). Here, IOP = 15 mmHg.

4.1. Effect of Model Coupling

The coupled and uncoupled models predict significantly different levels of intraluminal pressure directly upstream and downstream of the microcirculation compartments (i.e., $P_{1,2}$ and $P_{4,5}$, as shown in Fig. 2(A)). These differences result from differing model assumptions: in the uncoupled model, $P_{4,5}$ is held fixed, while in the coupled model, the passive effects of IOP and compression of the lamina cribrosa on the diameters of the CRA and CRV cause $P_{1,2}$ and $P_{4,5}$ to change. In addition, in the uncoupled model, the change in pressure along the CRA (i.e., $\Delta P_{\mathrm{CRA}} = P_{in} - P_{1,2}$, as shown in Fig. 2(B)) is held constant at 22 mmHg based on previous model predictions.[22,23] To maintain this constant drop in pressure, resistance in the CRA must decrease significantly (as shown in Fig. 2(C)).

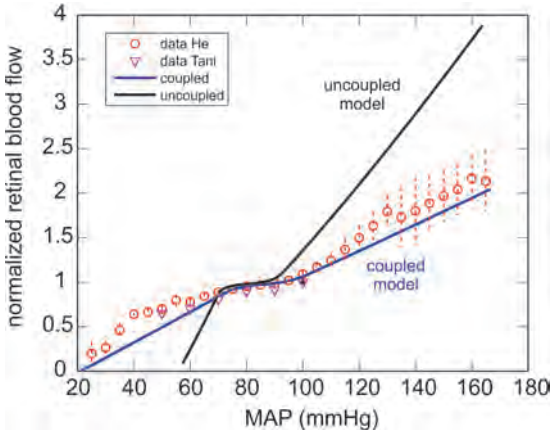

Fig. 5. Normalized values of blood flow predicted by the coupled model (blue curve) and uncoupled model (black curve) are compared with data from Refs. [7, 21] (red open markers) and Ref. [24] (magenta triangles) as MAP is varied between 20 and 165 mmHg for IOP = 10 mmHg.

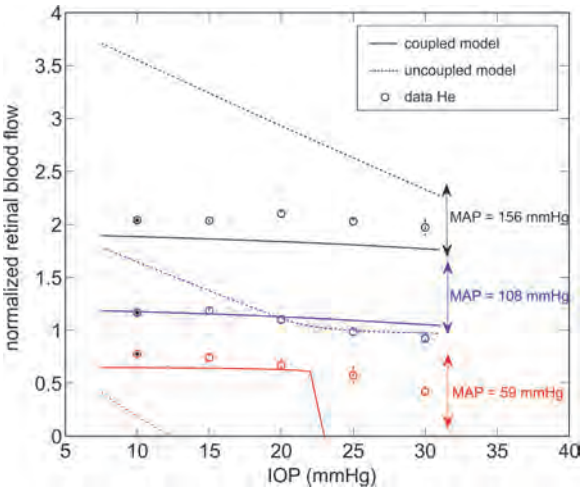

Fig. 6. Coupled (solid) and uncoupled (dashed) model predictions of normalized blood flow as IOP is varied between 7.5–31 mmHg are compared with experimental measures[7,21] at low-, normal- and elevated-blood pressure values corresponding to MAP = 59 (red), 108 (blue), and 156 mmHg (black), respectively. Note that these exact MAP values were provided by authors He et al. since average values were reported in Ref. [7]. All flow values are normalized with respect to the control state flow value for IOP = 15 mmHg and MAP = 93 mmHg.

In contrast, in the coupled model, the mechanical effects of IOP and the lamina cribrosa dictate ΔP_{CRA} and cause nonlinear changes in the CRA resistance. As MAP increases, the change in pressure along the CRA also increases and the resistance of the CRA decreases slightly. The coupled and uncoupled models were built to yield the same behavior in the control state, and thus the $P_{1,2}$ and $P_{4,5}$ values are the same for both models in the control state (as observed by the intersection of the curves at MAP = 93 mmHg in Fig. 2(A)). As MAP increases above the control state, ΔP_{CRA} is lower in the uncoupled model than the coupled model, and the reverse is true when MAP is decreased below the control state. Together, these relationships explain the differences in $P_{1,2}$ and $P_{4,5}$ predicted by the two models.

Blood flow and oxygen saturation also differ between the coupled and uncoupled models. While the two models predict nearly identical autoregulation plateaus (Fig. 3(A)), the change in flow outside the pressure range for autoregulation is more realistic in the coupled model, as evidenced by its agreement with experimental data (Fig. 5). In the uncoupled model, flow is predicted to approach zero at a higher value of MAP than in the coupled model. Flow will equal zero once $\Delta P = P_{1,2} - P_{4,5} = 0$. As can be seen in Figure 2(A), the curves for $P_{1,2}$ and $P_{4,5}$ in the uncoupled model intersect at a higher value of MAP than the coupled model, explaining the faster decline in flow as MAP decreases.

The differences in flow outside the autoregulation range for each model suggests that the assumptions in the uncoupled model are particularly relevant to studying

autoregulation while the model assumptions in the coupled model provide a more accurate description of the overall hemodynamic behavior of the vascular supply to the retina. Similarly, the ranges of venous saturation predicted by both models are nearly equivalent (Fig. 3(B)), but the coupled model does not yield as steep of a decline in venous saturation as MAP decreases since blood flow does not decrease as rapidly. From the results in Figure 4, it is also apparent that the combined action of the metabolic and carbon dioxide responses is important in achieving flow regulation.

4.2. Comparison with Experimental Measurements

Comparing both the uncoupled and coupled model predictions with experimental data[7,21,24] highlights the importance of including the mechanical effects of IOP and the lamina cribrosa when modeling blood supply to the retina. As shown in Figure 5, the coupled model provides a very close match to experimental measures of flow in the retina of the rat[7,21] and cat.[24] It is important to note that none of the data collected by He et al. or Tani et al.[24] was used in the formulation or parameter optimization of this model (for details on parameter estimation for this model, see Refs. [22, 23]); rather, the data set is only used to validate the model, and the agreement between theory and experiment highlights the value of including both a mechanical description of autoregulation and IOP in the model.

Figure 6 provides further evidence that coupling the macrocirculation and microcirculation models is necessary to provide an accurate description of blood flow to the retina. Model simulations for IOP = 7.5–31 mmHg at low, normal, and elevated MAP values are compared with experimental data.[7,21] As both the coupled model and experimental data show, flow is relatively constant (with a slight decrease) over this range of IOP values. The uncoupled model predicts a much more significant decrease in flow with IOP which deviates substantially from the collected data. This decrease is due to the fixed levels of $P_{1,2}$ and $P_{4,5}$ (given a specific IOP value) in the uncoupled model, which leads to a decrease in flow as resistance increases with IOP. He et al. provides measures for IOP as high as 110 mmHg, but both theoretical models are limited once IOP is increased beyond a certain threshold (leading to the closure of the small arterioles in the coupled model). The coupled model is also unable to provide predictions for values of MAP or IOP that cause $P_{4,5} = P_{\text{out}}$.

4.3. Summary

Although the model presented in this study does not specifically include the mechanical effects of IOP on retinal neurons, it incorporates a mechanistic model of the IOP effect on the deformation of the lamina cribrosa and vessel tone of the venous compartments, thereby including important mechanistic effects of IOP on blood flow supply to the entire retinal microcirculation. This is an important contribution to the understanding of retinal hemodynamics because it pinpoints mechanical elements of the system that lead to changes in flow. The relationships modeled by He et al.[7] are based on empirical relationships observed from experimental data collection, but they do not provide information on the contribution of individual mechanical factors of the system. Determining how to treat blood flow impairment under pathological conditions is very difficult based on empirical relationships but can be easier given theoretical models, such as the one presented here, that identify contributions of various mechanical and regulatory factors to be targeted (e.g., autoregulation mechanisms and the effect of IOP on the CRA, CRV, and lamina cribrosa).

The model presented by He et al.[7] quantifies the relationship between retinal function and OPP. This is a major step in retinal disease modeling since it relates how changes in flow and oxygenation may have a direct effect on retinal function. Although the retinal blood flow, tissue oxygen consumption, and oxygen extraction ratio can be calculated using the model presented in the current study, the model does not yet contain a means for determining the IOP-induced mechanical stress on neurons. A simple linear threshold model is implemented by He et al.,[7] but the threshold value for IOP at which mechanical stress affects neurons is optimized to be 50 mmHg, which is significantly higher than the values of IOP capable of being explored by the present model. The coupled model will be extended in future work to include a Starling resistor description for the venules and veins so that the model results can be related to data sets collected for higher IOP values.

In summary, this study demonstrates that the coupled model is necessary to yield a comprehensive and accurate depiction of hemodynamics in the retina and to obtain model predicted values of flow that are in good agreement with laser Doppler flowmetry measures in rats during MAP and IOP elevation. Elucidating the mechanisms involved in the ophthalmic disease process and the vascular contributions to these processes may provide new hope in identifying new treatment approaches in vision preservation.

References and Notes

1. L. Bonomi, G. Marchini, M. Marraffa, P. Bernardi, R. Morbio, and A. Varotto; Vascular risk factors for primary open angle glaucoma: The egna-neumarkt study; *Ophthalmology* 107, 1287 **(2000)**.
2. A. Harris, L. Kagemann, R. Ehrlich, C. Rospigliosi, D. Moore, and B. Siesky; Measuring and interpreting ocular blood flow and metabolism in glaucoma; *Canadian Journal of Ophthalmology Journal Canadien D'ophtalmologie* 43, 328 **(2008)**.
3. S. S. Hayreh; Blood flow in the optic nerve head and factors that may influence it; *Progress in Retinal and Eye Research* 20, 595 **(2001)**.
4. C. A. Hulsman, J. R. Vingerling, A. Hofman, J. C. Witteman, and P. T. de Jong; Blood pressure, arterial stiffness, and open-angle glaucoma: The Rotterdam study; *Archives of Ophthalmology* 125, 805 **(2007)**.
5. M. C. Leske, A. Heijl, L. Hyman, B. Bengtsson, L. Dong, and Z. Yang; Predictors of long-term progression in the early manifest glaucoma trial; *Ophthalmology* 114, 1965 **(2007)**.

6. D. Moore, A. Harris, D. Wudunn, N. Kheradiya, and B. Siesky; Dysfunctional regulation of ocular blood flow: A risk factor for glaucoma? *Clin Ophthalmol* 2, 849 **(2008)**.
7. Z. He, J. K. Lim, C. T. Nguyen, A. J. Vingrys, and B. V. Bui; Coupling blood flow and neural function in the retina: A model for homeostatic responses to ocular perfusion pressure challenge; *Physiological Reports* 1, e00055, **(2013)**.
8. P. Jeppesen, C. Aalkjaer, and T. Bek; Myogenic response in isolated porcine retinal arterioles; *Current Eye Research* 27, 217 **(2003)**.
9. C. Delaey and J. Van de Voorde; Pressure-induced myogenic responses in isolated bovine retinal arteries; *Investigative Ophthalmology and Visual Science* 41, 1871 **(2000)**.
10. T. Nagaoka and A. Yoshida; Noninvasive evaluation of wall shear stress on retinal microcirculation in humans; *Investigative Ophthalmology and Visual Science* 47, 1113 **(2006)**.
11. D. M. Collins, W. T. McCullough, and M. L. Ellsworth; Conducted vascular responses: Communication across the capillary bed; *Microvascular Research* 56, 43 **(1998)**.
12. M. L. Ellsworth; The red blood cell as an oxygen sensor: What is the evidence? *Acta Physiologica Scandinavica* 168, 551 **(2000)**.
13. A. Alm and A. Bill; The oxygen supply to the retina II, Effects of high intraocular pressure and of increased arterial carbon dioxide tension on uveal and retinal blood flow in cats, A study with radioactively labelled microspheres including flow determinations in brain and some other tissues; *Acta Physiologica Scandinavica* 84, 306 **(1972)**.
14. F. Maingret, M. Fosset, F. Lesage, M. Lazdunski, and E. Honore; TRAAK is a mammalian neuronal mechano-gated K+channel; *J. Biol. Chem.* 274, 1381 **(1999)**.
15. F. B. Kalapesi, J. C. H. Tan, and M. T. Coroneo; Stretch-activated channels: A mini-review. Are stretch-activated channels an ocular barometer? *Clin. Exp. Ophthalmol.* 33, 210 **(2005)**.
16. A. Kloda, L. Lua, R. Hall, D. J. Adams, and B. Martinac; Liposome reconstitution and modulation of recombinant *N*-methyl-*D*-aspartate receptor channels by membrane stretch; *P. Natl. Acad. Sci. USA* 104, 1540 **(2007)**.
17. A. Alm and A. Bill; Blood flow and oxygen extraction in the cat uvea at normal and high intraocular pressures; *Acta Physiol. Scand.* 80, 19 **(1970)**.
18. J. T. Ernest; Autoregulation of optic-disk oxygen tension; *Investigative Ophthalmology and Visual Science* 13, 101 **(1974)**.
19. J. B. HIckam and R. Frayser; Studies of the retinal circulation in man: Observations on vessel diameter, arteriovenous oxygen difference, and mean circulation time; *Circulation* 33, 302 **(1966)**.
20. R. A. Linsenmeier and L. Padnick-Silver; Metabolic dependence of photoreceptors on the choroid in the normal and detached retin; *Investigative Ophthalmology and Visual Science* 41, 3117 **(2000)**.
21. Z. He, C. T. Nguyen, J. A. Armitage, A. J. Vingrys, and B. V. Bui; Blood pressure modifies retinal susceptibility to intraocular pressure elevation; *PloS One* 7, e31104 **(2012)**.
22. G. Guidoboni, A. Harris, S. Cassani, J. Arciero, B. Siesky, A. Amireskandari, L. Tobe, P. Egan, I. Januleviciene, and J. Park; Intraocular pressure, blood pressure, and retinal blood flow autoregulation: A mathematical model to clarify their relationship and clinical relevance; *Investigative Ophthalmology and Visual Science* 55, 4105 **(2014)**.
23. J. Arciero, A. Harris, B. Siesky, A. Amireskandari, V. Gershuny, and A. Pickrell, G. Guidoboni; Theoretical analysis of vascular regulatory mechanisms contributing to retinal blood flow autoregulation; *Investigative Ophthalmology and Visual Science* 54, 5584 **(2013)**.
24. T. Tani, T. Nagaoka, S. Nakabayashi, T. Yoshioka, and A. Yoshida; Autoregulation of retinal blood flow in response to decreased ocular perfusion pressure in cats: Comparison of the effects of increased intraocular pressure and systemic hypotension; *Investigative Ophthalmology and Visual Science* 55, 360 **(2014)**.
25. G. Guidoboni, A. Harris, L. Carichino, Y. Arieli, and B. A. Siesky; Effect of intraocular pressure on the hemodynamics of the central retinal artery: A mathematical model; *Mathematical Biosciences and Engineering: MBE* 11, 523 **(2014)**.
26. B. C. Fry, T. K. Roy, and T. W. Secomb; Capillary recruitment in a theoretical model for blood flow regulation in heterogeneous microvessel networks; *Physiological Reports* 1, e00050 **(2013)**.